

A molecular dynamics study of bubble nucleation on grooved surfaces: Effects of wettability and heat flux

Mian Yu(余绵), Bingheng Li(李丙衡), Lianfeng Wu(吴连锋), Lianxiang Ma(马连湘), Xiangwen Meng(孟祥文), and Yuanzheng Tang(唐元政)

Citation: Chin. Phys. B, 2025, 34 (**11**): 114703. DOI: 10.1088/1674-1056/ae0896
http://cpb.iphy.ac.cn; http://iopscience.iop.org/cpb

What follows is a list of articles you may be interested in

Stable nanobubbles on ordered water monolayer near ionic model surfaces

Luyao Huang(黄璐瑶), Cheng Ling(凌澄), Limin Zhou(周利民), Wenlong Liang(梁文龙), Yujie Huang(黄雨婕), Lijuan Zhang(张立娟), Phornphimon Maitarad, Dengsong Zhang(张登松), and Chunlei Wang(王春雷)

Chin. Phys. B, 2025, 34 (**1**): 014701. DOI: 10.1088/1674-1056/ad989d

Molecular dynamics simulation of the flow mechanism of shear-thinning fluids in a microchannel

Gang Yang(杨刚), Ting Zheng(郑庭), Qihao Cheng(程启昊), and Huichen Zhang(张会臣)

Chin. Phys. B, 2024, 33 (**4**): 044701. DOI: 10.1088/1674-1056/ad08a7

A study of cavitation nucleation in pure water using molecular dynamics simulation

Hua Xie(谢华), Yuequn Xu(徐跃群), and Cheng Zhong(钟成)

Chin. Phys. B, 2022, 31 (**11**): 114701. DOI: 10.1088/1674-1056/ac588a

Molecular dynamics simulations on the wet/dry self-latching and electric fields triggered wet/dry transitions between nanosheets: A non-volatile memory nanostructure

Jianzhuo Zhu(朱键卓), Xinyu Zhang(张鑫宇), Xingyuan Li(李兴元), and Qiuming Peng(彭秋明)

Chin. Phys. B, 2022, 31 (**2**): 024703. DOI: 10.1088/1674-1056/ac3811

Comparative investigation of microjetting generated from monocrystalline tin surface and polycrystalline tin surface under plane impact loading

Shao-Wei Sun(孙少伟), Guan-Qing Tang(汤观晴), Ya-Fei Huang(黄亚飞), Liang-Zhi Cao(曹良志), and Xiao-Ping Ouyang(欧阳晓平)

Chin. Phys. B, 2021, 30 (**10**): 104701. DOI: 10.1088/1674-1056/abeeea

---

SPECIAL TOPIC — Heat conduction and its related interdisciplinary areas

A molecular dynamics study of bubble nucleation on grooved surfaces: Effects of wettability and heat flux

Mian Yu(余绵)[1], Bingheng Li(李丙衡)[1], Lianfeng Wu(吴连锋)[2], Lianxiang Ma(马连湘)[1], Xiangwen Meng(孟祥文)[1,†], and Yuanzheng Tang(唐元政)[1,‡]

[1] *College of Electromechanical Engineering, Qingdao University of Science and Technology, Qingdao* 266061, *China*
[2] *State Key Laboratory of Marine Coatings, Marine Chemical Research Institute Co., Ltd., Qingdao* 266071, *China*

(Received 16 July 2025; revised manuscript received 9 September 2025; accepted manuscript online 18 September 2025)

Bubble nucleation plays a crucial role in boiling heat transfer and other applications. Traditional experiments struggle to capture its microscopic mechanisms, making molecular dynamics simulations a powerful tool for such studies. This work uses molecular dynamics simulations to investigate bubble nucleation of water on copper surfaces with sinusoidal groove roughness under varying heat flux and surface wettability. Results show that at the same wettability, higher heat flux leads to higher surface temperatures after the same heating time, promoting bubble nucleation, growth, and departure. Moreover, under constant heat flux, stronger surface hydrophilicity enhances heat transfer from the solid to the liquid, further accelerating the nucleation. This study provides valuable insights into the mechanism of bubble nucleation and offers theoretical guidance for enhancing heat transfer.

Keywords: molecular dynamics, bubble nucleation, wettability conditions, heat flux

PACS: 47.11.Mn, 47.55.dd, 68.35.Ct, 61.30.Hn

DOI: 10.1088/1674-1056/ae0896 **CSTR:** 32038.14.CPB.ae0896

1. Introduction

The bubble nucleation, growth, and detachment behaviors in the nucleate boiling regime play a decisive role in heat transfer. The disturbances caused by the bubbles lead to a dramatic increase in the heat transfer coefficient and heat flux during boiling heat transfer,[1] which is why it is widely applied in industrial heat exchangers,[2–5] gas release,[6–8] aerospace,[9–11] biomedical applications,[12–14] nuclear cooling,[15–17] and food and chemical industries,[18–20] among other fields.

In the study of bubble behavior, traditional experimental methods primarily observe and measure the process of bubble formation in liquids through physical experiments. However, due to limitations in scale and observation, traditional experiments struggle to precisely control and observe microscopic processes that occur in extremely small spaces and over very short timescales, making it difficult to reveal the microscopic mechanisms of bubble nucleation. In contrast, molecular dynamics simulations can calculate physical quantities such as the temperature, volume, and pressure of the simulated system by considering the interactions and movements between atoms and molecules. This allows for a precise depiction of the entire process of bubble nucleation at the atomic and molecular scale, providing deep insights into the conditions for bubble nucleation, the effects of external factors on the nucleation process, and helping us to understand the microscopic mechanisms behind bubble nucleation. Molecular dynamics research on the microscopic phenomena and mechanisms of bubble nucleation has provided new theoretical support and practical guidance for the optimization of bubble nucleation, making it an important tool in the study of bubble nucleation. Pang[21] employed molecular dynamics simulations to model the pool boiling process on surfaces with different structured grooves. The results indicated that an arrayed grooved surface significantly improved heat transfer efficiency during the boiling process by altering the nucleation position and morphology of the bubbles. Specifically, on surfaces with wider grooves, bubbles formed earlier and at the bottom of the grooves, while on surfaces with narrower grooves, bubble formation occurred slightly later and at the top of the grooves. Miao and Xia[22] constructed nanocanals with structured surfaces to investigate the effect of nanostructure depth on flow boiling. The results found that the grooves induced bubble nucleation, mainly because the presence of cavities allowed the internal argon atoms to absorb extra energy from the surrounding wall and get closer to the heating layer. The reduction in solid thermal resistance led to increased heat transfer efficiency, resulting in earlier bubble nucleation and a stronger tendency for nucleation to occur within the cavities. The above studies mainly focus on the impact of surface roughness on bubble nucleation. In addition, wettability conditions are also a significant factor

†Corresponding author. E-mail: meng_qust2013@163.com
‡Corresponding author. E-mail: tangyuanzheng@163.com

© 2025 Chinese Physical Society and IOP Publishing Ltd. All rights, including for text and data mining, AI training, and similar technologies, are reserved.

affecting bubble nucleation. Miao *et al.*[23] used molecular dynamics methods to study the bubble nucleation process of liquid in a nanoscale channel on a solid wall. They analyzed the effect of wall wettability on bubble nucleation and growth. The results showed that as the wettability of the wall increases, the time for homogeneous nucleation is advanced. Zhao[24] employed molecular dynamics simulations to investigate the impact of mixed hydrophilic–hydrophobic wettability surfaces on the boiling heat transfer performance of water films. The study found that when the area of the strongly wetting region accounts for 60% to 70% of the total surface area, the maximum heat flux is achieved; furthermore, the bubble nucleation time is close to that on a completely strongly wetting surface. This indicates that strong wettability conditions can promote bubble nucleation and enhance boiling heat transfer. Liu *et al.*[25] used molecular dynamics simulations to study the effect of mixed wettability columnar nanostructures on the boiling heat transfer performance of a nanometric argon film on a copper plate. The study showed that compared to a purely hydrophilic wall, increasing the hydrophobic ratio changed the solid–liquid interface properties, which caused the liquid to begin boiling earlier. Zhou *et al.*[26] studied the bubble nucleation process of liquid argon on nanostructured surfaces with different wettabilities. The study found that the location of bubble nucleation depended on the wettability of the columns. When the columns were hydrophilic, bubble nucleation occurred in most of the fluid, while when the columns were hydrophobic, bubble nucleation occurred on the column surfaces. Bai[27] established a three-dimensional surface potential model to explore the relationship between wettability, surface potential, and boiling heat transfer. The study found that water molecules on hydrophilic surfaces have higher temperature gradients and initial heat flux compared to those on hydrophobic surfaces, as well as shorter boiling initiation times and lower interface thermal resistance. This indicates that hydrophilic surfaces are favorable for enhancing rapid boiling heat transfer. Liu *et al.*[28] used non-equilibrium molecular dynamics simulations to study the nanoscopic liquid–gas phase transition process of argon on solid copper substrates with different surface wettabilities and roughness. The study found that increased wettability of argon on solid copper surfaces enhances the heat transfer between solid and fluid atoms, as well as increases the evaporation mass flux of liquid argon. The bubble nucleation time also occurred earlier with the increase in wettability. Yin[29] used molecular dynamics simulations to study the mechanism of nanofluids in boiling heat transfer. The results showed that because nanoparticles can improve the thermal conductivity of the liquid, increase the frequency of bubble nucleation, and enhance the bubble departure velocity, the introduction of nanofluids can significantly improve boiling heat transfer performance. Wang[30] studied the wettability characteristics of nanofluids and their role in enhancing boiling heat transfer. The study found that compared to base fluids, nanoparticles enhance boiling heat transfer, and hydrophilic particles provide a more significant enhancement effect compared to hydrophobic particles.

Molecular dynamics studies on bubble behavior have revealed that surface roughness and wettability significantly influence bubble dynamics. Heat transfer research indicates that pits, crevices, and cavities on heated walls are the most likely nucleation sites for vaporization, making them a fundamental focus in the engineering development of enhanced boiling heat transfer.[1] However, existing molecular dynamics studies have rarely explored bubble nucleation, coalescence, and disturbances within adjacent pits. To address this gap, this study investigates the bubble behavior of water on a copper surface with closely spaced dual-groove structures while considering the effect of surface wettability. Additionally, most molecular dynamics studies have stimulated bubble behavior by controlling the temperature of the heated wall. However, in practical applications such as industrial heat transfers and electronic device cooling, boiling heat transfer typically occurs under constant heat flux conditions. Therefore, this study employs a constant heat flux on the heated wall to induce phase change in water. This research examines bubble nucleation, growth, and coalescence on dual-groove structures under different surface heat flux and wettability conditions. It identifies variations in bubble nucleation sites and morphologies, as well as single- and multi-bubble behaviors. Furthermore, through statistical analyses of number density, volume, temperature, and temperature distribution, this study elucidates the influence of surface heat flux and wettability on bubble behavior and the underlying microscopic mechanisms.

2. Simulation methods

As shown in Fig. 1, the simulated atomic model system consists of three parts: the copper atoms of the upper plate, the copper atoms of the lower plate, and the water molecules between the two plates. The simulation system includes 6679 water molecules and 5832 copper atoms, totaling 25869 atoms, forming a rectangular domain with dimensions of 122.69 Å, 20.00 Å, and 520.00 Å in the x, y, and z directions, respectively. The copper atoms are arranged in a face-centered cubic (FCC) lattice with a lattice constant of 3.61 Å. The undulating dual-groove structure on the bottom copper wall along the x-direction is constructed based on the following sine function:

$$f(x) = h_0 + A\sin(2\pi x/p), \tag{1}$$

where h_0 represents the distance to the z-axis, A is the amplitude, and p is the period.[31] Beneath the sinusoidal grooves, a substrate composed of six layers of 2592 copper atoms is

present. Among them, the bottom three layers of copper atoms are fixed to prevent atomic displacement or penetration during the heating process. The upper three layers are subjected to a heat flux, serving as the heat source to induce the phase transition of water. Throughout all simulation stages, a fixed boundary condition is applied in the negative z-direction, while periodic boundary conditions are implemented in all other directions.

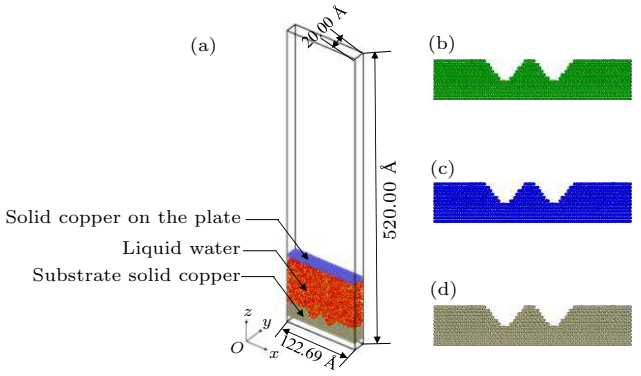


Fig. 1. Initial configuration of the simulation domain. (a) Overall model diagram. (b) Bottom copper atoms under hydrophobic conditions. (c) Bottom copper atoms under middle conditions. (d) Bottom copper atoms under hydrophilic conditions.

The interaction force between copper atoms is represented by van der Waals (vdW) forces and described using the Lennard–Jones (L-J) potential function

$$\phi_{(r_{ij})} = 4\varepsilon\left[\left(\frac{\sigma}{r_{ij}}\right)^{12} - \left(\frac{\sigma}{r_{ij}}\right)^{6}\right], \quad r \le r_{\text{cut}}, \tag{2}$$

where ε is the energy parameter, σ is the distance parameter, r_{ij} is the distance between atoms i and j, and r_{cut} is the cutoff radius. Additionally, to ensure that all copper atoms vibrate only around their initial positions and to prevent deformation of the sinusoidal groove structure, an elastic force is applied to the copper atoms:[32]

$$F = -Kr, \tag{3}$$

where $K = 52$ N/m is the elastic constant, and r is the displacement of an atom relative to its initial position. The interactions between water molecules are described using the SPC/E model, which effectively captures the physical and chemical properties of water molecules[33,34] and is a widely-used classical water model in molecular dynamics simulations. In this model, the charges of the oxygen (O) and hydrogen (H) atoms in the water molecule are $q_O = -0.8476e$ and $q_H = 0.4238e$, respectively. The Coulombic long-range interactions are calculated using the particle-particle-particle-mesh (PPPM) solver.[35] The intermolecular forces between water molecules are described through the O–O interaction. To save computational time while maintaining accuracy, the SHAKE algorithm[36] is applied to constrain the O–H bond length and the H–O–H angle in the water molecules, ensuring they remain rigid. The wettability conditions are determined by the intermolecular interaction forces between water molecules and copper atoms and are adjusted by modifying the L-J potential function parameters:

$$\phi_{(r_{ij})} = 4\varepsilon'\left[\left(\frac{\sigma'}{r_{ij}}\right)^{12} - \left(\frac{\sigma'}{r_{ij}}\right)^{6}\right], \quad r \le r_{\text{cut}}, \tag{4}$$

$$\varepsilon' = \varepsilon\beta^2, \tag{5}$$

$$\sigma' = \beta^{-1/6}\sigma. \tag{6}$$

Here, β is the parameter used to adjust the interface wettability conditions, and ε' and σ' are the modified energy and distance parameters, respectively. The potential energy parameters for this study are listed in Table 1. The water contact angle (CA) on the copper substrate is calculated by the density profile of a cylindrical water droplet on smooth bare surface.[37,38] When $\varepsilon_{\text{O-Cu}}$ is set to 3.685 meV ($\sigma_{\text{O-Cu}} = 0.338$ nm), a CA of approximately 120° is achieved and indicates a hydrophobic wetting condition. Furthermore, a CA of approximately 87.3° is obtained for a middle wetting condition when $\varepsilon_{\text{O-Cu}}$ is set to 7.37 meV ($\sigma_{\text{O-Cu}} = 0.319$ nm), which is close to the experimental value of 85.9° and simulation value of 84.1° in a previous study.[37] Lastly, for hydrophilic wetting conditions, setting $\varepsilon_{\text{O-Cu}}$ to 14.74 meV ($\sigma_{\text{O-Cu}} = 0.3011$ nm) yields a CA of close to 4.7°.

Table 1. Parameters of H_2O and Cu.

Atom pairs	σ (nm)	ε (meV)
Cu–Cu	0.2377	409.3
O–O	0.3166	6.739
O–Cu (hydrophobic)	0.3380	3.685
O–Cu (middle)	0.3190	7.370
O–Cu (hydrophilic)	0.3011	14.740

In this study, the piston-assisted pressure control method is employed to maintain the pressure stability of the simulation system.[39] Specifically, the copper plate at the top is set as a movable piston, and an external force is applied to each atom along the z-direction to maintain pressure equilibrium, thereby preventing pressure fluctuations from interfering with or affecting the bubble behavior. The external force applied to each atom in the upper copper plate is determined by the following equation:

$$F_{\text{atom}} = \frac{F_{\text{total}}}{N_{\text{up}}} = \frac{P \cdot S_{xoy}}{N_{\text{up}}}, \tag{7}$$

where F_{total} is the total external force applied to the upper copper plate, N_{up} is the number of atoms in the upper copper plate, $P = 1$ bar is the set pressure, and S_{xoy} is the area of the projection of the top plate onto the xoy plane. The setup enables bubble evolution under an approximately constant-pressure environment. Although the periodic boundary conditions impose some degree of spatial constraint, the top plate has sufficient

room to move upward, preventing the bubble size from being significantly affected by finite-size effects.

In this study, molecular dynamics simulations are performed on the entire system, excluding the fixed copper atoms at the bottom, which are divided into two stages: the relaxation process and the heating process. The relaxation process lasts for 1 ns, during which the microcanonical (NVE) ensemble combined with the Langevin[40] thermostat is used to stabilize the temperature of the simulation system at 298 K. In the heating process, the system equilibrium is controlled by the microcanonical (NVE) ensemble, and heat flux is applied to the copper atoms in the heat source region, inducing a temperature rise that leads to bubble formation. The duration of the heating process varies with the wettability conditions: under hydrophilic conditions, bubbles are observed after 1 ns of heating, whereas under hydrophobic conditions, the heating process must last for 2 ns. To comprehensively study the phenomena and mechanisms of bubble dynamic evolution during the heating process, the temperature, density, and trajectory data of the atoms are statistically analyzed every 1 ps. The heat flux applied to the copper atoms in the heat source region and the calculated wall heat flux during the heating process are shown in Table 2.

Table 2. Heat flow applied to the heat source and the calculated heat flux.

System	Heat flow (W)	Heat flux ($W \cdot m^{-2}$)
#1	5.00×10^{-7}	1.77×10^{10}
#2	5.60×10^{-7}	1.97×10^{10}
#3	8.01×10^{-7}	2.82×10^{10}

The molecular dynamics simulations in this study are conducted using LAMMPS software,[41] with the atomic equations of motion numerically integrated using the Verlet algorithm and a time step of 1 fs. To analyze bubble nucleation, growth, and their dynamic behaviors, atomic trajectory and other data are visualized and analyzed using the Open Visualization Tool (OVITO)[42] and Visual Molecular Dynamics (VMD)[43] software.

3. Results and discussion

This study employs the aforementioned model and simulation methods to investigate the bubble behavior of water on a dual-groove copper surface under nine different scenarios, considering three different surface wettabilities and three heat flux. In this section, the dynamic process of bubble nucleation is analyzed through the calculation of density distributions, temperature changes, temperature distributions, and bubble volume changes. The study explores the influence patterns and mechanisms of wettability and heat flux on the bubble nucleation behavior.

As shown in Fig. 2, snapshots of the bubble growth process on the bottom copper substrate surface under different heat flux are displayed for various wettability conditions. It is evident that under hydrophobic conditions, at the initial mo-

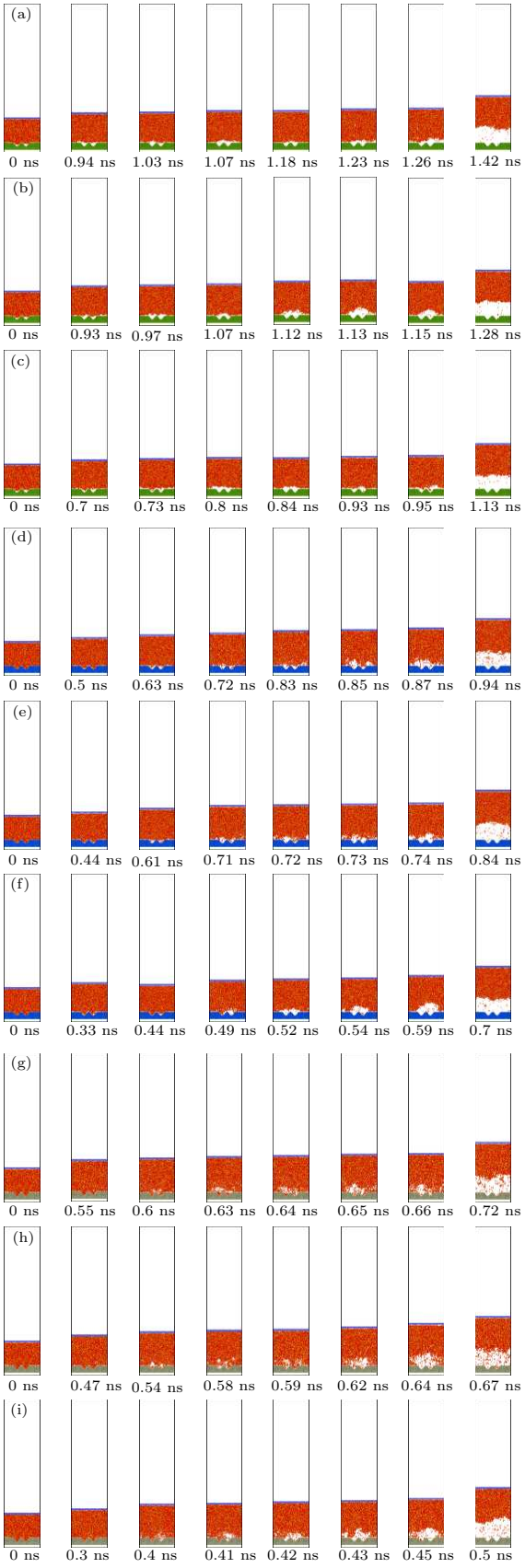


Fig. 2. Snapshot of bubble nucleation in a simulated system. Hydrophobic conditions: (a) heat flux #1, (b) heat flux #2, (c) heat flux #3. Middle conditions: (d) heat flux #1, (e) heat flux #2, (f) heat flux #3. Hydrophilic conditions: (g) heat flux #1, (h) heat flux #2, (i) heat flux #3.

ment when the liquid water comes into contact with the bottom copper substrate, it cannot completely wet the substrate surface. This phenomenon corresponds to the Cassie model.[44] This occurs because, under hydrophobic conditions, the intermolecular interactions are reduced,[45] thus preventing complete wetting of the copper substrate. However, this does not affect the research results. In contrast, under middle and hydrophilic conditions, the water molecules are able to fully wet the bottom copper substrate surface at 0 ns, corresponding to the Wenzel model.[44] Furthermore, in Figs. 2(a)–2(c), it can be observed that under hydrophobic conditions, as the simulation progresses, water molecules begin to undergo irregular thermal motion due to heating. The volume of the water region expands, and the upper copper plate moves upward to maintain pressure stability within the system. At three different heat flux (from small to large), small bubbles form at 1.03 ns, 0.97 ns, and 0.73 ns in the liquid phase. These bubbles continue to grow and eventually form stable bubble nuclei at 1.23 ns, 1.13 ns, and 0.93 ns. With continuous heating, the bubble nuclei grow into a steam film, which gradually detaches from the bottom copper substrate surface. Under middle and hydrophilic conditions, figures 2(d)–2(i) show that as the heating region begins to heat under middle conditions, bubbles form at 0.63 ns, 0.61 ns, and 0.44 ns at three different heat flux, respectively. These bubbles continue to grow and eventually form stable bubble nuclei at 0.85 ns, 0.73 ns, and 0.54 ns. Subsequently, a steam film forms and detaches from the bottom copper surface. Under hydrophilic conditions, bubbles form at 0.6 ns, 0.54 ns, and 0.4 ns for the three different heat flux, respectively. These bubbles continue to grow and form stable bubble nuclei at 0.65 ns, 0.62 ns, and 0.43 ns. A steam film subsequently forms and detaches from the bottom copper surface. The results show that with increasing heat flux in the heating region, the time at which bubble nuclei form is advanced. Hydrophilic conditions also significantly promote the nucleation of bubbles and the formation and detachment of the steam film.

When bubbles are generated in the liquid water region, a decrease in the number of water molecules in that area is observed, leading to a reduction in local density.[46] To better understand the bubble nucleation process, the number density of water molecules in the region above the bottom copper substrate groove within a 36.4 Å range was statistically analyzed, and the variation in the number density of water molecules over time was plotted, as shown in Fig. 3. Under hydrophilic conditions, the decrease in the number density of water molecules occurs the fastest, which indicates that bubble nucleation and growth happen the earliest, with the most pronounced growth trend. This is because hydrophilic surfaces have strong adsorption properties, which effectively lower the energy barrier required for bubble nucleation,[47] thus facilitating bubble nucleation and growth. Under hydrophobic conditions, the decrease in the number density of water molecules is slower, and the bubble nucleation occurs the latest. This is due to the weaker interaction between hydrophobic surfaces and water molecules, requiring a higher energy barrier for bubble nucleation, and leading to a delayed nucleation time. The figure also shows that heat flux is another key factor affecting bubble nucleation. Under high heat flux (heat flux #3) conditions, the number density of water molecules decreases the fastest, indicating that bubble nucleation occurs more rapidly, and the rate of bubble evaporation is also the fastest. The bubbles form a steam film earlier and detach from the bottom copper substrate surface sooner. In the combination of high heat flux and hydrophilic conditions, the number density of water molecules decreases the fastest, indicating that the joint effect of high heat flux and hydrophilic surfaces significantly promotes bubble nucleation and growth.

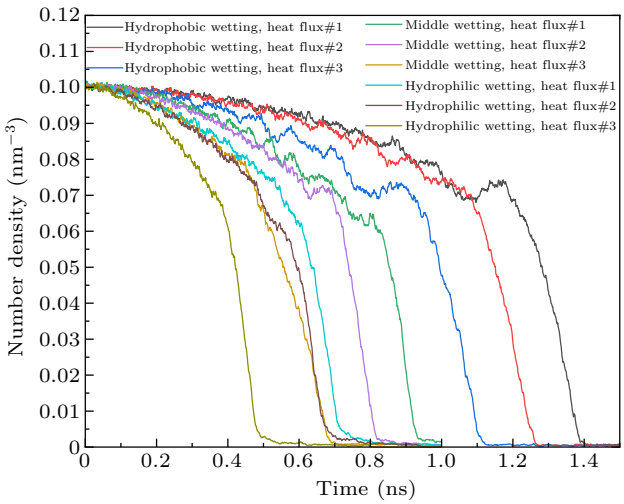


Fig. 3. Density variation with time in the statistical region.

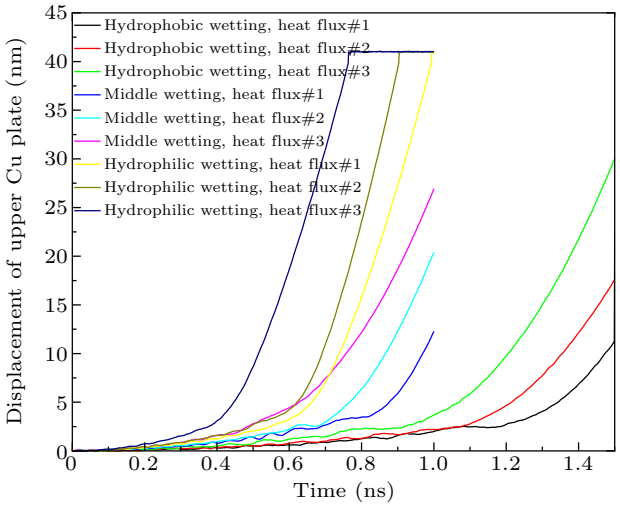


Fig. 4. Variation of the upper plate displacement over time.

As the bubbles gradually form and grow, the upper plate continues to move upward. The displacement of the upper plate can clearly reflect the changes in bubble growth. To

analyze this, the displacement of the upper plate over time was statistically examined, and the resulting plot of the upper plate displacement versus time is shown in Fig. 4. At the initial stage of heating, the curve for the upper plate displacement rises slowly, indicating a small displacement. This corresponds to the stage where water molecules are undergoing random thermal motion. When bubbles form, the displacement curve of the upper plate shows a distinct inflection point, marking the transition to the phase where the bubbles grow into stable bubble nuclei. During this stage, the displacement of the upper plate increases rapidly. Subsequently, as the bubble nuclei grow into a steam film and detach from the bottom copper substrate surface, the upper plate continues to move upward. From the overall results, it is clear that when the heat flux is the same, as the surface wettability changes from hydrophobic to hydrophilic, the displacement of the upper plate increases, and the inflection point appears earlier. Similarly, when the wettability conditions are consistent, increasing the heat flux leads to a faster displacement of the upper plate, with the inflection point also occurring earlier.

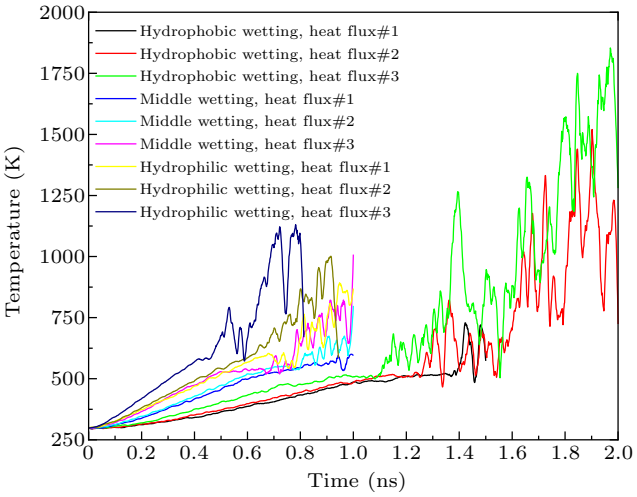


Fig. 5. Temperature variation of H_2O in the statistical region with time.

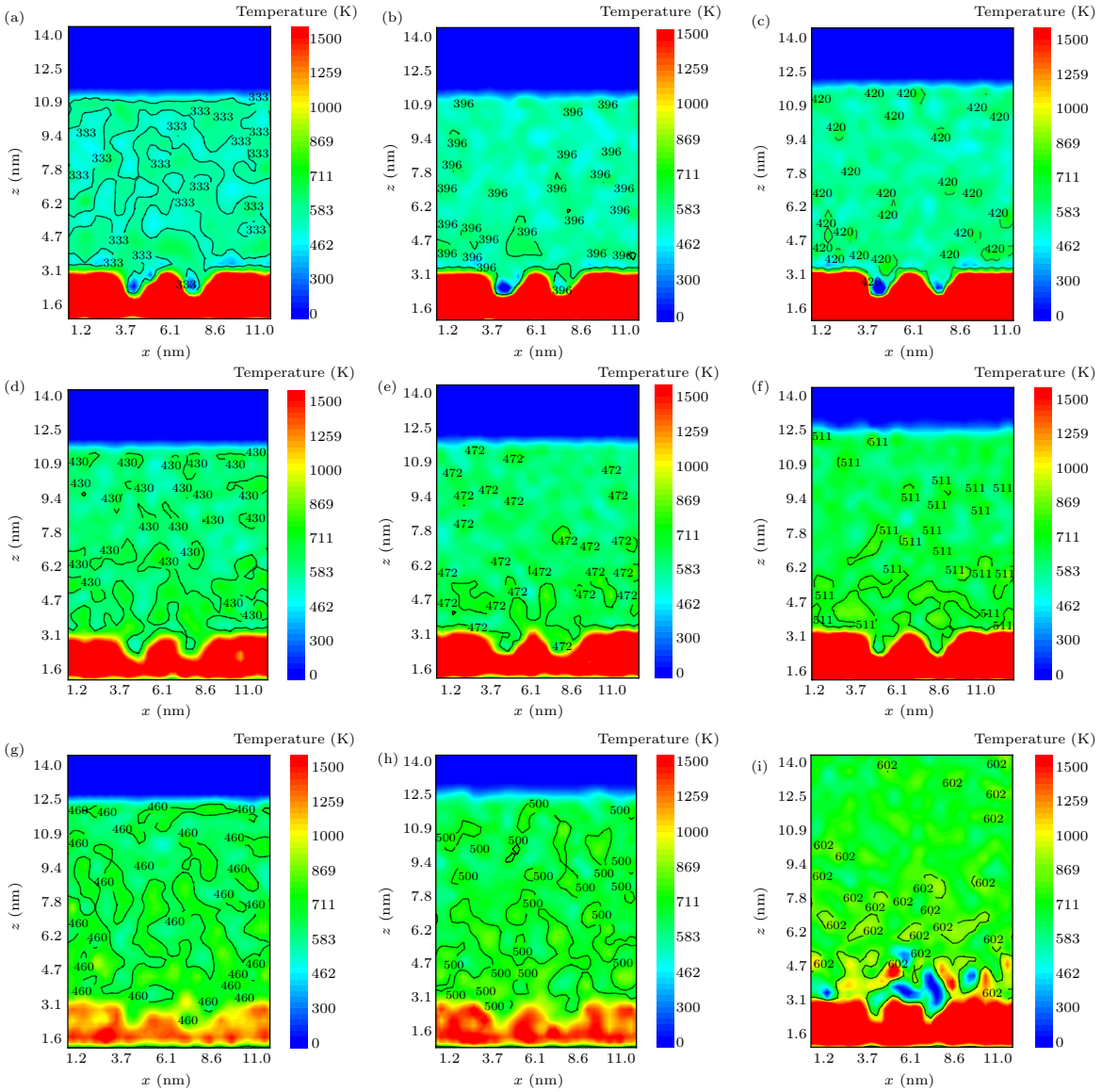


Fig. 6. Temperature distribution map at the same moment of 0.43 ns. Hydrophobic wetting: (a) heat flux #1, (b) heat flux #2, (c) heat flux #3. Middle wetting: (d) heat flux #1, (e) heat flux #2, (f) heat flux #3. Hydrophilic wetting: (g) heat flux #1, (h) heat flux #2, (i) heat flux #3.

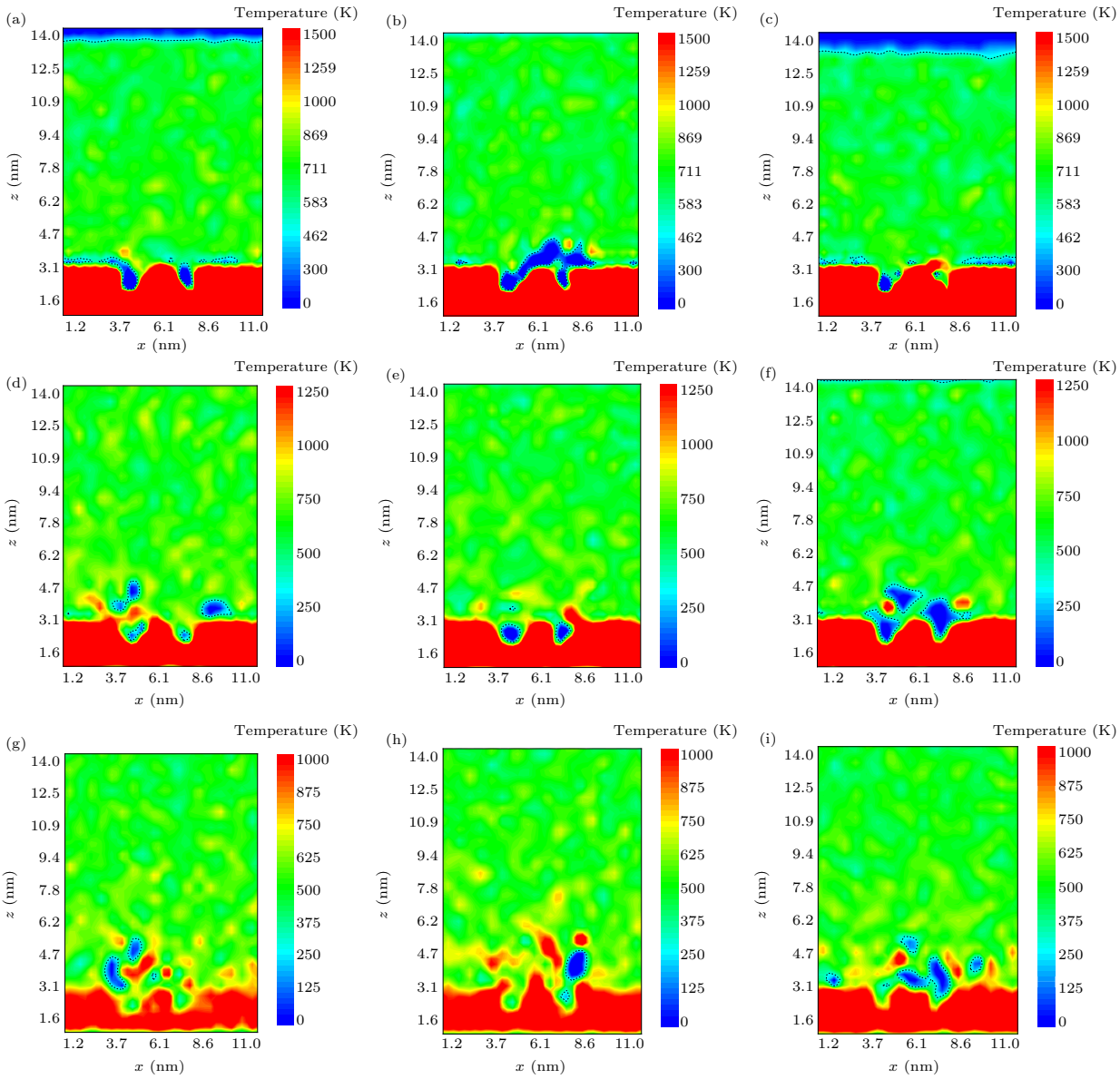


Fig. 7. Temperature distribution map at the moment of bubble nucleation stabilization. Hydrophobic wetting: (a) heat flux #1, 1.23 ns; (b) heat flux #2, 1.13 ns; (c) heat flux #3, 0.93 ns. Middle wetting: (d) heat flux #1, 0.85 ns; (e) heat flux #2, 0.73 ns; (f) heat flux #3, 0.54 ns. Hydrophilic wetting: (g) heat flux #1, 0.65 ns; (h) heat flux #2, 0.62 ns; (i) heat flux #3, 0.43 ns.

The essence of bubble nucleation is the heat transfer from the bottom copper plate to the liquid water molecules, and the efficiency of this heat transfer directly influences the formation and growth of the bubbles. To analyze this process, the temperature in the nucleation region was monitored, and its change over time was plotted, as shown in Fig. 5. Under the maximum heat flux (#3), the temperature increase in the water molecule region shows the steepest slope, and the temperature quickly reaches its maximum simulated value.[48] In contrast, under the minimum heat flux (#1), the temperature increase in the water molecule region is slower. Additionally, the wettability conditions also have a significant impact on the temperature change of the water molecule region. Under hydrophilic conditions, the temperature increase is more rapid, and the slope of the temperature increase curve is steeper. Under hydrophobic conditions, the temperature increase is slower compared to both middle and hydrophilic conditions. This indicates that a higher heat flux leads to a faster temperature increase in the water molecule region. Moreover, hydrophilic conditions significantly enhance the heat transfer from the bottom copper plate to the liquid water molecules.

We performed a statistical analysis of the temperature at the same time point (0.43 ns) for all nine simulations and created a temperature distribution map, as shown in Fig. 6. Under the same wettability conditions, when the heat flux increases, the temperature of the bottom copper substrate is higher, and the temperature in the water molecule region is also higher. This indicates that, at the same time point, a higher heat flux leads to more heat being transferred from the bottom copper substrate to the water molecule region, thereby promoting bubble nucleation.

When a stable bubble nucleus forms in the water molecule

region, the temperature distribution between the bottom copper substrate and the water molecules varies according to different conditions, as shown in Fig. 7. Under hydrophobic conditions, the bottom copper substrate temperature is higher, while under hydrophilic conditions, the bottom copper substrate temperature is the lowest. Compared to middle and hydrophilic surfaces, hydrophobic surfaces weaken the intermolecular interactions between liquid water molecules and the bottom copper substrate,[49] thereby hindering heat transfer and leading to greater heat accumulation within the copper region. In contrast, middle and hydrophilic surfaces transfer heat more effectively to the liquid water region, leading to a higher temperature in the liquid water area. This also provides strong evidence that hydrophilic surfaces can promote bubble nucleation, as the heat transfer to the liquid water region is more efficient, resulting in higher temperatures in the liquid and facilitating the formation of bubbles.

The most critical factor influencing bubble nucleation is the heat transfer between Cu and H_2O, which can be elucidated in terms of the Kapitza resistance

$$R_{\mathrm{K}} = \frac{T_2 - T_1}{q}, \tag{8}$$

where T_2 represents the average temperature of the top three layers of Cu atoms on the bottom, T_1 represents the average temperature of the selected liquid H_2O molecules adjacent to the solid surface, and q is the heat flux from the solid surface to the liquid. As shown in Fig. 8, the Kapitza resistance exhibits an obvious dependence on the varying wettability. As the surface hydrophilicity becomes stronger, the Kapitza resistance decreases and the heat transfer efficiency is improved, resulting in the enhancement of bubbles on a hydrophilic surface.

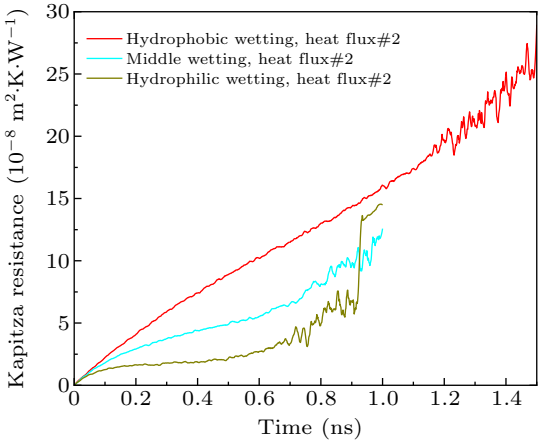


Fig. 8. Variation of the Kapitza resistance between the bottom plate and liquid.

To better investigate the growth pattern of bubble nucleation in the double-groove simulation system, we compared it with the bubble nucleation process in a single-groove simulation system. The results are as follows. By comparing Fig. 9 with Figs. 2(c), 2(e), and 2(f), it can be observed that in the single groove, bubbles always nucleate first at the bottom of the groove and grow as a single bubble until they reach the top of the groove and span across it, eventually forming a vapor layer. In the double-groove structure, each groove independently generates a bubble nucleus, and each nucleus grows independently to the top of its groove before merging, after which the bubble continues to grow. Both experimental and MD studies indicate that surface grooves serve as the primary nucleation sites, and increasing the number of grooves creates more effective nucleation sites. Furthermore, since the bottom of the groove is the core region for heat transfer, providing a highly superheated environment favorable for bubble nucleation, the increase in the groove number significantly promotes bubble nucleation. Results from the number density variation of water molecules in the statistical region, the displacement of the top plate, and the temperature variation of water molecules in the statistical region all indicate that the double-groove simulation system facilitates the bubble growth process.

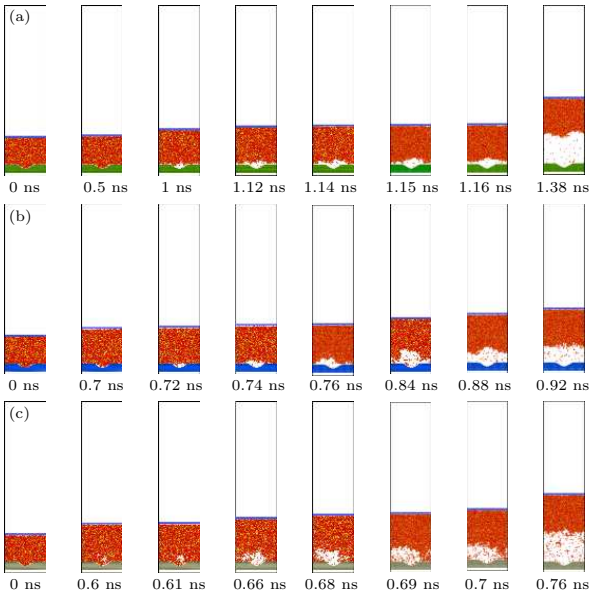


Fig. 9. Snapshots of bubble nucleation in the single-groove simulation system under heat flux #2. (a) Hydrophobic, (b) middle, and (c) hydrophilic wetting conditions.

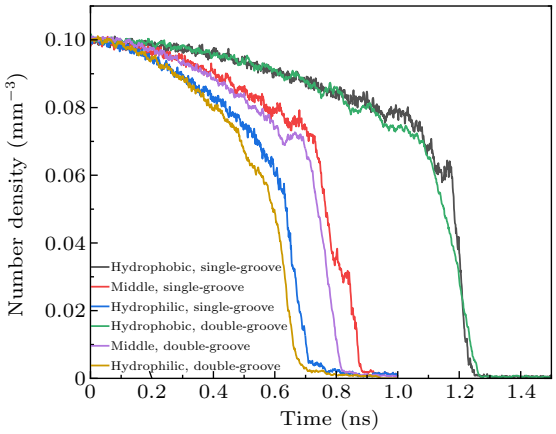


Fig. 10. Temporal variation of water molecule number density in the statistical region during bubble nucleation for single- and double-groove systems under heat flux #2.

We statistically analyzed the energy during the bubble nucleation process in the double-groove simulation system under heat flux #2 and middle wettability, and plotted the energy distribution at corresponding time points, as shown in Fig. 13. During the initial stages of bubble nucleation and growth, the energy in the regions where bubbles form is relatively high, and the local energy continues to increase as the bubbles grow. When the simulation reaches approximately 0.75 ns, bubble coalescence across grooves occurs, and it can be clearly observed that the system energy significantly decreases due to the merging of bubbles. Meanwhile, the coalescence process is accompanied by local liquid backflow, resulting in rewetting. These results indicate that bubble coalescence not only alters the local thermodynamic state but also has a significant impact on nucleation kinetics through energy reduction and rewetting effects, revealing the unique physical significance of multi-bubble interactions in double-groove structures.

Finally, we summarize all the results by statistically analyzing the time at stable bubble nuclei and the bubble nucleation rate, as shown in Figs. 14 and 15. Since the system pressure is constant, the displacement of the top plate can effectively reflect the state of bubble growth. Additionally, as the bottom plate is fixed, the change in the product of the top plate's upward displacement and the bottom surface area of the system approximately represents the change in bubble volume during the growth process. The bubble growth rate is defined as the ratio of the change in bubble volume from the initial bubble appearance to the formation of a continuous vapor layer to the corresponding time required. It is evident that as the heat flux increases, the time for stable bubble nucleus formation is significantly advanced. Additionally, the enhancement of hydrophilic conditions also noticeably promotes bubble nucleation. This highlights the combined effect of increased heat flux and improved wettability in accelerating the bubble nucleation process.

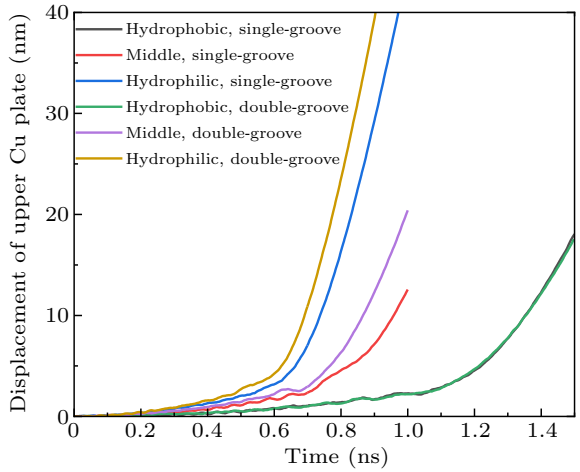


Fig. 11. Temporal variation of the top plate displacement during bubble nucleation for single- and double-groove systems under heat flux #2.

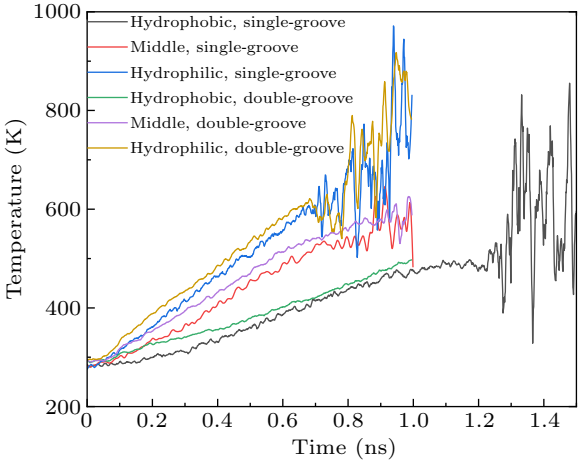


Fig. 12. Temporal variation of water molecule temperature in the statistical region during bubble nucleation for single- and double-groove systems under heat flux #2.

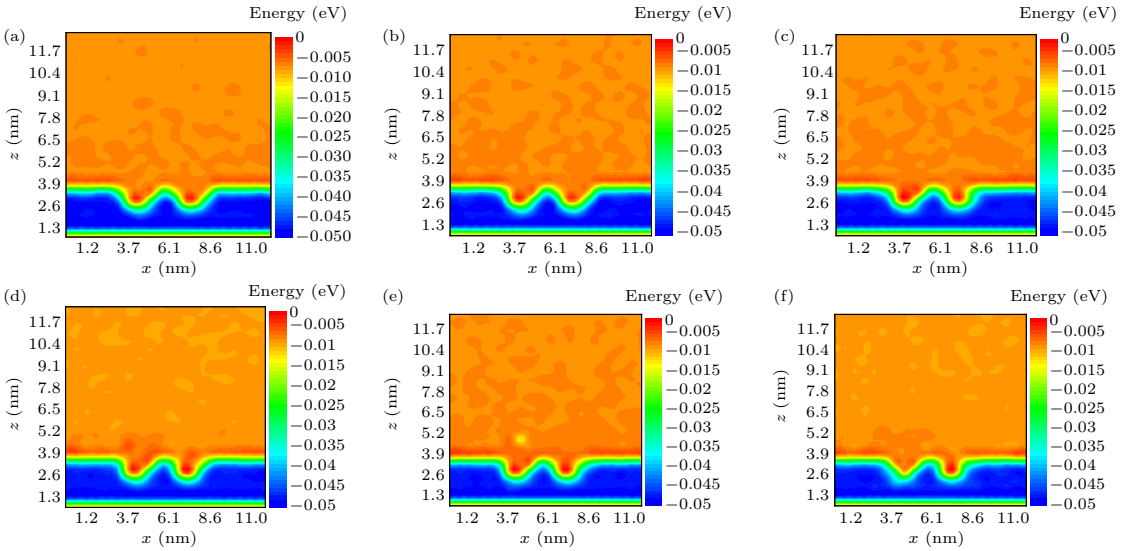


Fig. 13. Energy distributions at different time points during the bubble nucleation process: (a) at 0.65 ns, (b) at 0.7 ns, (c) at 0.72 ns, (d) at 0.73 ns, (e) at 0.74 ns and (f) at 0.75 ns.

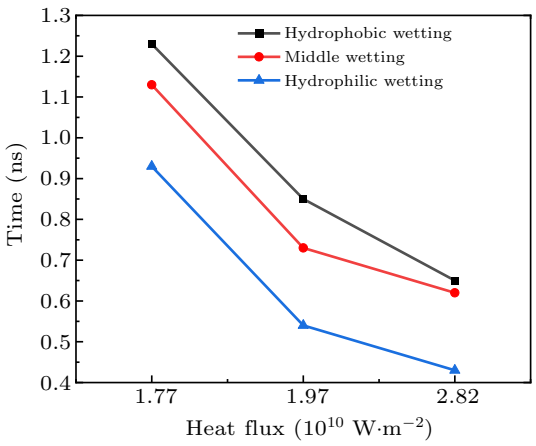


Fig. 14. Stable bubble formation time under different heat flux and wetting conditions.

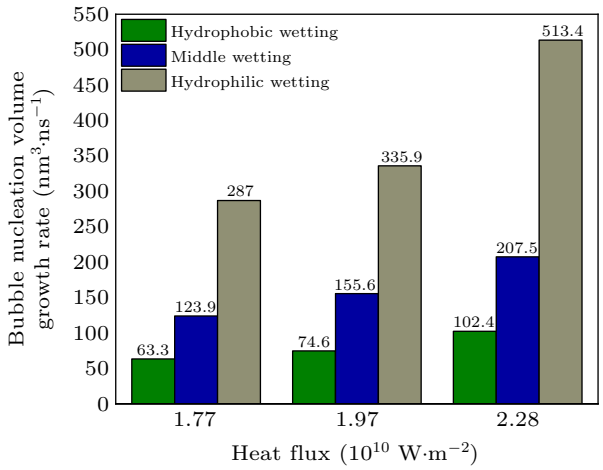


Fig. 15. Bubble nucleation volume growth rate.

4. Conclusions

This study employs molecular dynamics simulations to investigate the bubble behavior of water on a copper substrate with a sinusoidal double-groove rough surface. By applying a constant heat flux to the substrate, the effects of different wettability conditions and heat fluxes on bubble nucleation and growth were observed. The micro-mechanism of bubble behavior was explained through temperature distribution analysis. The results are summarized as follows. (i) As the hydrophilic conditions increase, the interaction between the copper substrate and water molecules strengthens, significantly promoting bubble nucleation, and the growth rate becomes faster. (ii) Heat flux directly influences the local temperature of the copper substrate and water molecules, thereby determining the bubble nucleation process. A higher heat flux provides sufficient heat more quickly, causing bubbles to form earlier and grow faster. The results bridge the microscopic and macroscopic insights on bubble behaviors in nucleate boiling.

Acknowledgment

Project supported by the National Natural Science Foundation of China (Grant No. 52176077) .

References

[1] Yang S M and Tao W Q 2006 *Heat Transfer* 4th Edn. (Beijing: Higher Education Press) p. 316 (in Chinese)
[2] Ma Z Y, Zhang L T, Bu S S, Sun W, Chen D Q and Pan L M 2019 *Prog. Nucl. Energy* **112** 135
[3] Al Omari S A B, Bashir A A K Al Hammadi M I, Al Hamalawi F J, Elnajjar E and Ghazal A M 2017 *Int. Commun. Heat Mass Transfer* **86** 71
[4] Zhang Y H, L D Gu, Wang Z Y, Fu X L, Cao Q and Yang Y H 2017 *Appl. Therm. Eng.* **114** 186
[5] Kang M G 2018 *Exp. Therm. Fluid Sci.* **97** 375
[6] Chakraborty P, Tonks M R and Pastore G 2014 *J. Nucl. Mater.* **452** 95
[7] Evans J H, Galindo R E and van Veen A 2003 *Nuclear Inst. Meth. Phys. Res. B* **217** 276
[8] Zhang N X, Daniel O, Liu J H and Khellil S 2024 *Heat Transfer Eng.* **45** 433
[9] Wang J X, Yu B B, Qian C Y, Shi J Y and Chen J P 2023 *Therm. Sci. Eng. Prog.* **45** 102150
[10] He Y C, Hu C Z, Jiang B, Sun Z H, Ma J, Li H Y and Tang D W 2022 *Fuel* **324** 124778
[11] Vieira G C, Flórez M J P and Mantelli M B H 2020 *Int. J. Heat Mass Transfer* **156** 119832
[12] Kulik A V, Mokrin S N, Kraevskii A M, Minaev S S, Guzev M A and Chudnovskii V M 2024 *Tech. Phys. Lett.* **50** 198
[13] Kohany T B, Arogeti M, Malka A and Sher E 2023 *Energies* **16** 6763
[14] Chudnovskii V M, Yusupov V I, Dydykin A V, Nevozhai V I, Kisilev A Y, Zhukov S A and Bagratashvili V N 2017 *Quantum Electron.* **47** 361
[15] Reiss C, Gerschenfeld A and Colin C 2024 *Nucl. Eng. Des.* **428** 113453
[16] Mokos A, Patel R A, Karalis K, Churakov SV and Prasianakis N I 2024 *Int. J. Heat Mass Transfer* **230** 125747
[17] Jin-Seong Y, Won L C, Heepyo H, Hyukjae K, Hyun K J, Geon-Woo K, Goon-Cherl P and Kyu C H 2024 *Appl. Therm. Eng.* **236** 121906
[18] Wang D H and Guo Z Y 2020 *New J. Chem.* **44** 4529
[19] Aghajanzadeh S, Sultana A, Ziaiifar A M and Khalloufi S 2024 *Food Res. Int.* **188** 114494
[20] Jesús M L, Renato M A, Andrea M, Sudheera Y, Mariana H M, John G, Onur A, Sergi G S and E M E 2023 *J. Plant Interact* **18** 2271492
[21] Pang R Y 2023 *Molecular dynamics study of pool boiling on arrayed groove surfaces* (M.S. Thesis) (Tianjin: Hebei University of Technology) (in Chinese)
[22] Miao S S and Xia G D 2024 *J. Mol. Liq* **400** 124457
[23] Miao R C, Zhang S Z, Chen Z X and Li Y 2020 *Chem. Ind. Eng. Prog.* **39** 1641
[24] Zhao H 2020 *Molecular dynamics simulation study on the effect of hydrophobic-hydrophilic mixed wettability surface on water film boiling heat transfer* (M.S. Thesis) (Beijing: North China Electric Power University) (in Chinese)
[25] Liu F R, Chen Z X and Li Y H 2024 *J. At. Mol. Phys.* **41** 032001
[26] Zhou W J, Zhang Y H and Wei J J 2022 *Langmuir* **38** 1223
[27] Bai P 2022 *Molecular dynamics study of the effects of surface roughness and wettability on boiling* (Ph.D. Dissertation) (Beijing: North China Electric Power University) (in Chinese)
[28] Liu H Q, Deng W, Ding P and Zhao J Y 2021 *Nucl. Eng. Des.* **382** 111400
[29] Yin X Y 2020 *Mechanism of boiling heat transfer enhancement in nanofluids by molecular dynamics simulation* (Ph.D. Dissertation) (Dalian: Dalian University of Technology) (in Chinese)
[30] Wang Z 2022 *Molecular dynamics study on wettability characteristics and enhanced boiling heat transfer mechanism of nanofluids* (Ph.D. Dissertation) (Shanghai: University of Shanghai for Science & Technology) (in Chinese)
[31] Vladislav A Y, Guillaume A and Molinari J F 2014 *Tribol. Lett.* **56** 171
[32] Deng W, Ma S H, Li W M, Liu H Q and Zhao J Y 2022 *Int. J. Heat Mass Transfer* **191** 122856
[33] Berendsen H J C, Grigera J R and Straatsma T P 1987 *J. Phys. Chem.* **91** 6269
[34] Kusalik P G and Svishchev I M 1994 *Science* **265** 1219
[35] Hockney R W and Eastwood J W 2021 *Computer Simulation Using Particles* (1st edn) (Boca Raton: CRC Press) pp. 267–269

[36] Ryckaert J P, Ciccotti G and Berendsen H J C 1977 *J. Comput. Phys.* **23** 327
[37] Rafiee J, Mi X, Gullapalli H, Thomas A V, Yavari F, Shi Y, Ajayan P M and Koratkar N 2012 *Nat. Mater.* **11** 217
[38] Isaiev M, Burian S, Bulavin L, Gradeck M, Lemoine F and Termentzidis K 2016 *Mol. Simul.* **42** 910
[39] Guo C, Ji C, Kong Y L, Liu Z G and Guo L 2023 *Materials* **16** 1984
[40] Schneider T and Stoll E 1978 *Phys. Rev. B* **17** 1302
[41] Steve P 1995 *J. Comput. Phys.* **117** 1
[42] Stukowski A 2010 *Modell. Simul. Mater. Sci. Eng.* **18** 015012
[43] Humphrey W, Dalke A and Schulten K 1996 *J. Mol. Graphics* **14** 33
[44] Zhang K, Yang J S and Huai X L 2024 *Int. J. Heat Mass Transfer* **224** 125323
[45] Wen S Z and Huang P 2011 *Interface Science and Technology* (1st edn) (Beijing: Tsinghua University Press) pp. 65–66 (in Chinese)
[46] Zhang L Y and Xu J L 2022 *J. Mol. Liq.* **366** 120272
[47] Ge S and Chen M 2013 *Acta Phys. Sin.* **62** 110204 (in Chinese)
[48] Kim D E, Yu D I, Jerng D W, Kim M H and Ahn H S 2015 *Exp. Therm. Fluid Sci.* **66** 173
[49] Wang Z Q, Wang P Y, Song H and Chen Z 2022 *J. Mol. Liq.* **347** 118360